Quantum spin Hall and quantum valley Hall effects in trilayer graphene and their topological structures

Majeed Ur Rehman[1,2,†] and A A Abid[1,2]

[1] ICQD, Hefei National Laboratory for Physical Sciences at Microscale, Department of Physics, University of Science and Technology of China, Hefei 230026, China

[2] Key Laboratory of Geospace Environment (Chinese Academy of Sciences), Department of Geophysics and Planetary Science, University of Science and Technology of China, Hefei 230026, China

(Received 28 April 2017; revised manuscript received 31 August 2017; published online 20 October 2017)

The present study pertains to the trilayer graphene in the presence of spin orbit coupling to probe the quantum spin/valley Hall effect. The spin Chern-number $\mathcal{C}_s$ for energy-bands of trilayer graphene having the essence of intrinsic spin–orbit coupling is analytically calculated. We find that for each valley and spin, $\mathcal{C}_s$ is three times larger in trilayer graphene as compared to single layer graphene. Since the spin Chern-number corresponds to the number of edge states, consequently the trilayer graphene has edge states, three times more in comparison to single layer graphene. We also study the trilayer graphene in the presence of both electric-field and intrinsic spin–orbit coupling and investigate that the trilayer graphene goes through a phase transition from a quantum spin Hall state to a quantum valley Hall state when the strength of the electric field exceeds the intrinsic spin coupling strength. The robustness of the associated topological bulk-state of the trilayer graphene is evaluated by adding various perturbations such as Rashba spin–orbit (RSO) interaction α_R, and exchange-magnetization M. In addition, we consider a theoretical model, where only one of the outer layers in trilayer graphene has the essence of intrinsic spin–orbit coupling, while the other two layers have zero intrinsic spin–orbit coupling. Although the first Chern number is non-zero for individual valleys of trilayer graphene in this model, however, we find that the system cannot be regarded as a topological insulator because the system as a whole is not gaped.

Keywords: trilayer graphene, quantum spin Hall effect, topological insulator, quantum phase transition

PACS: 73.43.–f, 73.20.–r, 85.75.–d, 73.43.Nq **DOI:** 10.1088/1674-1056/26/12/127304

1. Introduction

Symmetry is essential to classify different electronic states of matter. The Landau theory of the phase transition[1] is the key concept to differentiate the states of matter, this theory is based on the local order parameter. For example, ferro/paramagnetism and superconductivity/superfluidity states can be understood by the aforementioned principle. But after 1980, when the quantum Hall effect (QHE)[2,3] was discovered, the Landau theory failed to explain this new state of matter because the quantum Hall (QH) states, in principle, are distinct states but break no symmetry and hence cannot be explained under the shadow of the Landau theory of phase transition. So a new modified band theory was introduced known as topological band theory,[4] which takes the concept of topological invariants (Chern number) instead of the local order parameter. In principle, the QHE is the first example of a topological insulator (displaying insulating behavior in the bulk but has robust conducting channels at the edges).[5–7] The Chern-number can be expressed as an integral of a well-defined quantity known as the Berry curvature (analogous to magnetic field in electrodynamics) over the first Brillouin zone (BZ).[8]

In 1982, Using Kubo formalism, Thouless and his collaborators[8] made an efficacious attempt to link the topology (Chern-number) to the band structure of the two-dimensional band insulator having non-interacting electrons exposed to a strong magnetic field. The quantization of the Hall conductance in terms of Chern-number confirms the topological nature of the QH state; the edge channels cannot be removed unless the bulk band gap closes. Due to this major contribution, Thouless was awarded a Nobel prize in 2016. The next important development in the field was made by Haldane in 1988,[9] who came up with a theoretical model, where he demonstrated that one can think of topological protection without an applied magnetic field. It is in principle related to the composition of the band structure of materials. Initially, the citations of the Haldane model were very low because of its impractical realization but it increased rapidly after 2005, when Kane and his collaborator Male[10,11] presented a physical realization, for the first time, of the Haldane model by demonstrating that one can visualize the role of intrinsic spin–orbit (ISO) interaction as a magnetic field in the momentum space (momentum-space Berry curvatures), which has the opposite sign for opposite spins. This model introduced a new topological state requiring no external magnetic field and having spin current on the boundaries; this state of matter is now identified as quantum spin Hall (QSH) state[1,5,10–15] in the literature. Haldane was also awarded a noble prize shared with Thouless and Kosterlitz in 2016 for his contribution.

In this new electronic phase, called the quantum spin Hall effect (QSHE), the edge states are uniquely designed in the sense that they are insensitive to the non-magnetic pertur-

†Corresponding author. E-mail: majeedqau@live.com

© 2017 Chinese Physical Society and IOP Publishing Ltd

bations because of their helical nature (momentum and spin are locked with each other).[16] This phase preserves the time reversal (TR) symmetry and hence is known as a topological insulator. The topological invariant used to classify the QSH phases is known as Z_2 topological invariant[17] or spin Chern parity which can possess only two values $\nu = 0, 1$, where $0/1$ for an even/odd number of Kramer pairs at the boundaries.[18,19]

Impurities, which preserve the TR symmetry (non-magnetic impurities), do not posses the ability to back scatter the electrons, as for the reversal of momentum the flipping of spin is needed, which does not lie under the capacity of non-magnetic impurities.[20] The QSHE is observed only in those materials which have strong essence of intrinsic spin–orbit (ISO) coupling, but unfortunately the ISO coupling in graphene is so weak ($\sim 10^{-2}$ meV–10^{-3} meV[4,21,22]) that the quantum spin Hall (QSH) state is difficult to be observed experimentally in graphene and its layers, however the QSH state in graphene provides a good theoretical framework to observe this topological state in other two-dimensional (2D) materials having a strong essence of the spin–orbit coupling. In 2005, Molenkamp and his team were successful in the experimental confirmation of QSHE in HgTe quantum wells sandwiched between HgCdTe layers.[23,24] Another 2D material is known as silicene, which has strong SOC than graphene (and its layers) also hosts the QSH state.[25,26] In contrast to QSHE, the quantum-valley Hall effect (QVHE)[27–29] originates as a result of the broken space inversion-symmetry. In this quantum state of matter, Dirac-fermions that corresponds to different valleys, move to opposite transverse edges in the presence of an in-plane electric field. Recently, a great deal of attention has been paid to the topological insulators in the study of condensed matter physics,[30–41] because some new properties are believed to be extracted from it, which could be useful for technological usages, such as electronics, spintronics, valleytronics, and quantum computation.

In the present work, our aim is to study the trilayer graphene (ABC stacking) in the presence of intrinsic spin–orbit interaction (SOI) to probe QSHE while using a two-band Hamiltonian approach. Activation of spin index in the trilayer graphene introduces a new energy term in the Hamiltonian that corresponds to intrinsic SOI, this extra term gaps the spectrum in the bulk at the Dirac points with conducting spin-polarized edges. Unfortunately, this extra energy contribution is very small because of weak ISO interaction in the trilayer graphene[42] but recent development in this field shows that it can be strengthened by numerous means, such as curvature,[43] impurities[44] or Coulomb interaction,[45] this makes it possible to observe the QSH state. In addition, the QSHE in trilayer can be used as an approach to understand the coupling among three layers with each one having a topological nature. An attempt has been made to also discuss the topological configuration of the band structure of the trilayer graphene through the plotting of a three-dimensional (3D) unit vector on the unit sphere. Our consideration also revolves around the study of trilayer graphene in the presence of both ISO coupling and an applied electric field. Besides this, we have also incorporated a discussion regarding what happens when one considers a coupling between a metal and topological insulator. To do this, we present a theoretical model where only one of the outer layers has finite SOC while it is zero in the other two layers. This sort of tenability of the trilayer graphene is unrealizable because till now there has been no known way to tune the SO coupling in each sheet independently. However, this model provides a simple theoretical framework to understand SO proximity effects in other systems.[46] The stability of the QSH state against various perturbations such as Rashba SOI and exchange magnetization is also part of the discussion in this paper.

This paper is systematized as follows. In Section 2, we investigate the QSH effect in ABC trilayer layer graphene using the two-bands low energy approach and calculate the spin Chern-number for each valley and spin. Section 3 comprises discussions about the topological structure of the QSH state in the trilayer graphene. In Section 4, we highlight the main features of the trilayer graphene in the presence of both ISO coupling and perpendicular electric field. In Section 5, we examine the stability of the QSH state in the trilayer graphene against various perturbation terms such as Rashba spin–orbit (RSO) coupling α_{R} and Zeeman term M. In Section 6, we consider a theoretical model in which only one of the outer layers of the trilayer graphene has nonzero ISO coupling while the other two layers have zero ISO coupling. In the last section, we summarize our results and outcomes.

2. Model Hamiltonian

The band structure of ABC trilayer graphene is composed of six energy bands having cubic dispersion, two of them are gapless at the valley points $\boldsymbol{K}$ and $\boldsymbol{K}'$ (at zero energy) and are known as low energy bands, these bands originate as a result of coupling between A_1–B_3 sites, while the remaining four bands do not touch the Fermi surface and are known as high energy bands.[47] Since the strength of the ISO interaction in the trilayer graphene is weak, it cannot change the topology of the high energy bands. In other words, the contribution from high energy bands in the first Chern-number is very small so it is a convention to involve only the low energy states for the spin Chern-number calculations. So in the light of the above discussion we use effective 2×2 Hamiltonian[48] in our calculations. The two-level effective Hamiltonian of the ABC trilayer graphene in the basis $\{\psi^{\eta}_{A_1 s_z}, \psi^{\eta}_{B_3 s_z}\}$, can be modeled[42,48] as,

$$\mathcal{H}^{\eta}_{s_z}(p) = \mathcal{H}_{\mathrm{el}} + \mathcal{H}_{\mathrm{SO}}, \tag{1}$$

where $\mathcal{H}_{\mathrm{el}}$ ($\mathcal{H}_{\mathrm{SO}}$) corresponds to the electronic part (ISO interaction part), which is given by

$$\mathcal{H}_{\mathrm{el}} = \frac{v^3 p^3}{t_1^2}[\eta\cos(3\phi_p)\tau_x + \sin(3\phi_p)\tau_y], \tag{2}$$

$$\mathcal{H}_{\rm SO} = \alpha_{\rm so}\eta\tau_z s_z, \tag{3}$$

where $v = (\sqrt{3}/2)at$ is the Fermi velocity, $a = 1.42$ Å is the lattice constant of monolayer graphene, $t(t_1)$ describes the nearest neighbor intra-layer (strong inter-layer) coupling between A_j–B_j for $j = 1,2,3$ (B_1–A_2 and B_2–A_3), $\{\tau_i\}$, $i = 0,1,2,3$ represents the Pauli matrices in the space (A_1, B_3), η is the valley index which is $\eta = +1$ ($\eta = -1$) for valley $\boldsymbol{K}$ ($\boldsymbol{K}'$), s_z is the real spin index which is $s_z = +1$ ($s_z = -1$) for spin $\uparrow$ ($\downarrow$), $\alpha_{\rm so}$ is the strength of the ISO interaction, and $\boldsymbol{p} = p[\cos\phi_p, \cos\phi_p]$ is the momentum and $\phi_p = \tan^{-1}(p_y/p_x)$. In this model the spin is a good quantum number. Now to obtain the band dispersion relation, we diagonalize the above Hamiltonian,

$$E_n(p) = n\sqrt{\left(\frac{v^3p^3}{t_1^2}\right)^2 + \alpha_{\rm so}^2} = n\lambda(p), \tag{4}$$

where $n = \pm 1$ is the band index and

$$\lambda(p) = [(v^3p^3/t_\perp^2)^2 + \alpha_{\rm so}^2]^{1/2}.$$

We see that the system turns out to be gaped when the SO interaction is introduced. In addition, the energy does not depend on the spin index which ensures the TR symmetry in the system. In order to further investigate whether either this gaped system is a trivial or non-trivial band insulator, we calculate the first Chern number (winding number) for the said system. The Hamiltonian (1) can be modeled in terms of 3D unit vector $\hat{\boldsymbol{d}}(p)$ as,

$$\mathcal{H}_{s_z}^{\eta}(p) = \lambda(p)\left[\hat{d}_x(p)\tau_x + \hat{d}_y(p)\tau_y + \hat{d}_z(p)\tau_z\right], \tag{5}$$

where the three-component unit vector is defined as

$$\hat{\boldsymbol{d}}(p) = \left[\eta\delta(p)\cos(3\phi_p), \delta(p)\sin(3\phi_p), \hat{d}_z(p)\right]. \tag{6}$$

Here $\delta(p) = [1 - \hat{d}_z^2(p)]^{1/2}$ and $\hat{d}_z(p) = \eta s_z\alpha_{\rm so}/\lambda(p)$. The Chern-number (winding number) in terms of this unit vector for the 2×2 Hamiltonian (1) is given by[49–52]

$$\mathbb{C}(\eta, s_z) = \int \mathcal{F}(p)\,{\rm d}p_x{\rm d}p_y, \tag{7}$$

where $\mathcal{F}(p) = (1/4\pi)\left\{\left(\partial_{p_x}\hat{\boldsymbol{d}}(p)\times\partial_{p_y}\hat{\boldsymbol{d}}(p)\right)\cdot\hat{\boldsymbol{d}}(p)\right\}$. Physically, this number corresponds to how many times the 3D unit vector $\hat{\boldsymbol{d}}(p)$ covers the entire unit sphere upon covering the whole BZ. This is related to the topology of the band structure and may have different values for different band structures. The quantity $\mathcal{F}(p)$ can be calculated as

$$\mathcal{F}(p) = \chi_{\rm I} + \chi_{\rm II} + \chi_{\rm III} \tag{8}$$

with

$$\chi_{\rm I} = -\frac{3\eta}{p}\cos^2 3\phi_{\boldsymbol{p}}\delta(p)\partial_p\hat{d}_z(p),$$
$$\chi_{\rm II} = -\frac{3\eta}{p}\sin^2 3\phi\,\delta(p)\partial_p\hat{d}_z(p),$$
$$\chi_{\rm III} = -\frac{3\eta}{p}\left[\hat{d}_z(p)\right]^2\partial_p\hat{d}_z(p),$$

where, we have used,

$$\partial_{p_x}\hat{d}_x(p) = 3\eta\sin(3\phi_{\boldsymbol{p}})\delta(p)\beta_1 + \eta p\cos(3\phi_{\boldsymbol{p}})\partial_p\delta(p)\beta_2,$$
$$\partial_{p_y}\hat{d}_x(p) = -3\eta\sin(3\phi_{\boldsymbol{p}})\delta(p)\beta_2 + \eta p\cos(3\phi_{\boldsymbol{p}})\partial_p\delta(p)\beta_1,$$
$$\partial_{p_x}\hat{d}_y(p) = -3\cos(3\phi_{\boldsymbol{p}})\delta(p)\beta_1 + p\sin(3\phi_{\boldsymbol{p}})\partial_p\delta(p)\beta_2,$$
$$\partial_{p_y}\hat{d}_y(p) = 3\cos(3\phi_{\boldsymbol{p}})\delta(p)\beta_2 + p\sin(3\phi_{\boldsymbol{p}})\partial_p\delta(p)\beta_1,$$
$$\partial_{p_x}\hat{d}_z(p) = \partial_p\hat{d}_z(p)\,p\beta_2,$$
$$\partial_{p_y}\hat{d}_z(p) = \partial_p\hat{d}_z(p)\,p\beta_1,$$
$$\partial_{p_x}\phi_{\boldsymbol{p}} = -\beta_1,\ \ \partial_{p_y}\phi_{\boldsymbol{p}} = -\beta_2,\ \ \partial p_x = p\beta_2\partial_p,$$
$$\partial_{p_y} = p\beta_1\partial_p,\ \ \beta_{1(2)} = p_{y(x)}/p^2.$$

Now substituting Eq. (8) into Eq. (7),

$$\mathbb{C}(\eta, s_z) = \frac{3\eta}{4\pi}\int_0^\infty\int_0^{2\pi} p\,{\rm d}p\,{\rm d}\phi\,\frac{1}{p}\partial_p\hat{d}_z(p),$$
$$\mathbb{C}(\eta, s_z) = -\frac{3}{2}\eta\hat{d}_z(0) = -\frac{3}{2}s_z. \tag{9}$$

The total Chern-number can be calculated as

$$\mathcal{C} = \sum_{\eta=\pm1}\sum_{s_z=\pm1}(\mathbb{C}(\eta, s_z) = 0. \tag{10}$$

This ensures that the QSH state is a TR symmetrical electronic phase of the matter. Additionally, it ensures the fact that there exists zero charge current flowing on the boundaries of the said phase. Another interesting result can be seen by summing the contribution from both valleys for a given spin

$$\mathcal{C}_\uparrow = \sum_{\eta=\pm1}\mathbb{C}(\eta,\uparrow) = -3,\ \ \mathcal{C}_\downarrow = \sum_{\eta=\pm1}\mathbb{C}(\eta,\downarrow) = 3. \tag{11}$$

These results imply that the Chern-number for a given spin (up or down) has a quantized value, which is a justification of the statement that each filled band of a system having non-interacting electrons must have a quantized Chern-number.[53] The spin Chern-number plays the role of topological invariant for the systems having spin rotational symmetry about the z axis and is defined in the following fashion,[10,19]

$$\mathcal{C}_s = \sum_{i\epsilon{\rm occ}}\left(\frac{\mathbb{C}_\uparrow^{(i)} - \mathbb{C}_\downarrow^{(i)}}{2}\right), \tag{12}$$

where the summation runs over the occupied bands. Thus the spin Chern-number for our trilayer graphene system is $\mathcal{C}_s[= (\mathcal{C}_\uparrow - \mathcal{C}_\downarrow)/2] = -3$. Like the charge Hall conductivity, the spin Hall-conductivity can be written in terms of the spin Chern-number as,

$$\sigma_{xy}^s({\rm spin}) = \mathcal{C}_s\frac{e^2}{h} = -3\frac{e^2}{h}. \tag{13}$$

We see that the first Chern-number of the trilayer graphene is three times the single layer graphene, therefore accordingly the trilayer system has the edge channels, three times more than a single layer because the spin Chern-number corresponds to the number of Kramer pairs on a given edge of the sample.[18]

3. Topological structure of quantum spin Hall state in trilayer graphene

The topological configuration of the QSH state can be best visualized by looking at the plot of 3D unit vector $\hat{\boldsymbol{d}}(p)$ as a function of momentum $\boldsymbol{p}$ over a 3D unit sphere. Observing the structure of vector $\hat{\boldsymbol{d}}(p)$ on a unit sphere, one can extract some interesting physics in the form of topological objects, which we call triple-vortex merons. In topological terminology, the valley index η defines the vorticity (superfluidity analogy), $\eta = 1$ for right vortex and $\eta = -1$ for left vortex. The unit vector $\hat{\boldsymbol{d}}(p)$ depends on the index ηs_z, therefore we have four flavors which are

$$\eta s_z = \{(\boldsymbol{K},\uparrow),(\boldsymbol{K}',\uparrow),(\boldsymbol{K},\downarrow),(\boldsymbol{K}',\downarrow)\}.$$

In all flavors, at asymptotically large momentum, the z component of the unit vector $\hat{\boldsymbol{d}}(p)$ vanishes and thus it becomes confined to the x–y plane, i.e., winds around the equator of the unit sphere and displays vortex-like winding on the circle [see Fig. 1]. While in the vortex core, where the momentum is zero, the z component of the $\hat{\boldsymbol{d}}(p)$ becomes unity and we obtain, $\hat{\boldsymbol{d}}(p) = [0,0,\eta s_z]$. This shows that, in the vortex core the unit vector $\hat{\boldsymbol{d}}(p)$ points to the north pole of the unit sphere for $\{(\boldsymbol{K},\uparrow),(\boldsymbol{K}',\downarrow)\}$ while it points to the south pole in the flavors $\{(\boldsymbol{K},\downarrow),(\boldsymbol{K}',\uparrow)\}$. This clarifies that (i) for the flavors $\{(\boldsymbol{K},\uparrow),(\boldsymbol{K}',\downarrow)\}$, the mapping $\hat{\boldsymbol{d}}(p)$ starts to tilt gradually from the north pole towards the equator of the sphere as we increase the momentum, and is completely shifted to the x–y plane when the momentum becomes asymptotically large. In this way the unit vector $\hat{\boldsymbol{d}}(p)$ covers the upper hemisphere (three times) upon scanning the whole BZ. We call such a configuration triple-vortex merons with associated topological charge $\mathbb{C} = -3/2$ [see Figs. 1(a) and 1(c)]. (ii) Similarly, for the flavors $\{(\boldsymbol{K},\downarrow),(\boldsymbol{K}',\uparrow)\}$, the vector $\hat{\boldsymbol{d}}(p)$ starts to flip gradually from the south pole towards the equator of the 3D unit sphere, when we increase the momentum it is confined to the equator at asymptotically large momentum. This implies that the unit vector $\hat{\boldsymbol{d}}(p)$ scans the lower hemisphere upon covering the entire BZ. Thus the mapping $\hat{\boldsymbol{d}}(p)$ presents anti-triple-vortex meron-like configuration with associated topological charge $\mathbb{C} = 3/2$ [see Figs. 1(b) and 1(d)]. In principle, a meron is a half of a skyrmion having unit topological charge.[54] One more thing that is important to be noted is that unlike superfluids, where the vortex core has a singularity, these vortices do not have a singularity at the origin (vortex core).[50]

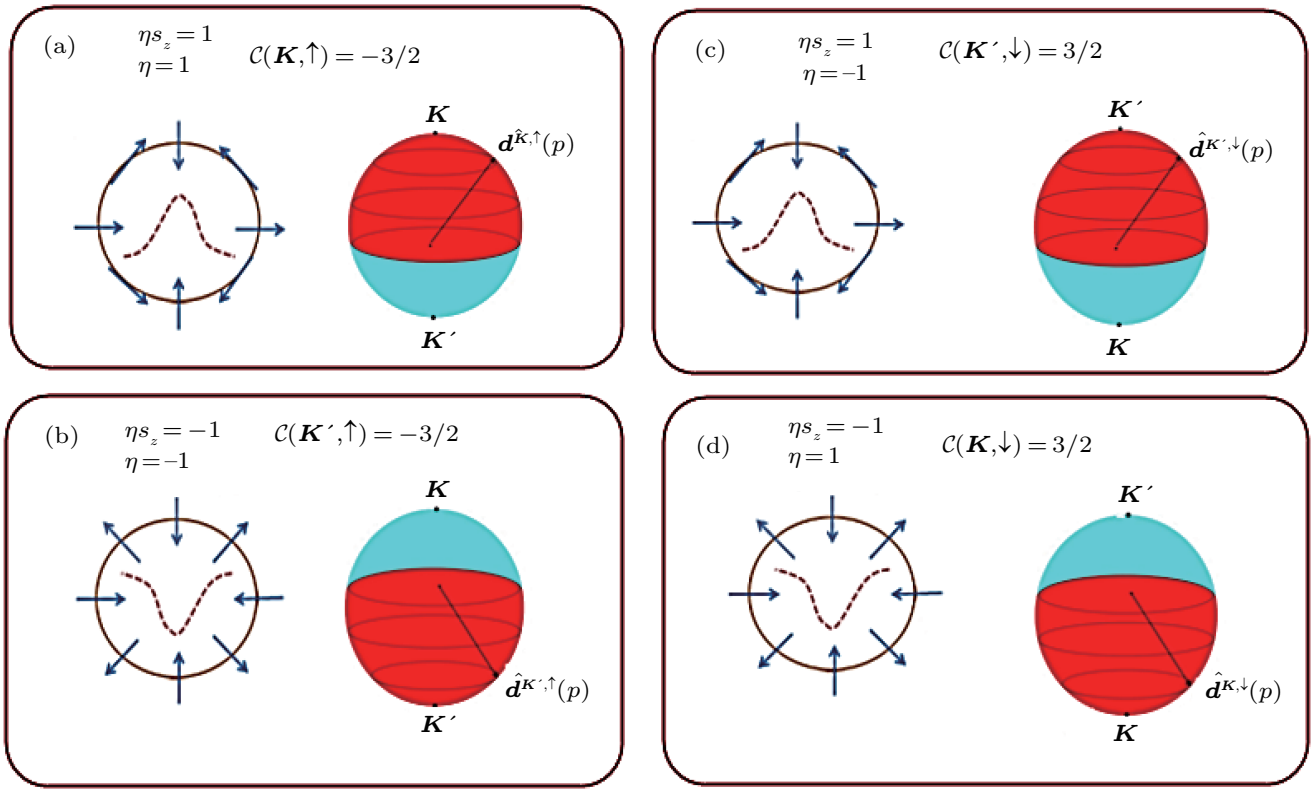


Fig. 1. (color online) Four flavors of triple-vortex merons. (a) Flavor with valley $\boldsymbol{K}$ and $\uparrow$: the unit vector $\hat{\boldsymbol{d}}(p)$ covers the upper hemisphere and displays a triple vortex meron-like configuration with associated topological charge $\mathcal{C}(\boldsymbol{K},\uparrow) = -3/2$. (b) Flavor with valley $\boldsymbol{K}'$ and $\uparrow$: $\hat{\boldsymbol{d}}(p)$ covers the lower hemisphere and displays a meron-like structure with $\mathcal{C}(\boldsymbol{K}',\uparrow) = -3/2$. (c) Flavor with valley $\boldsymbol{K}'$ and $\downarrow$: the mapping $\hat{\boldsymbol{d}}(p)$ covers the upper hemisphere and displays a triple vortex anti-meron-like configuration with associated topological charge $\mathcal{C}(\boldsymbol{K}',\downarrow) = 3/2$. (d) Flavor with valley $\boldsymbol{K}$ and $\downarrow$: $\hat{\boldsymbol{d}}(p)$ covers the lower hemisphere and displays an anti-meron-like structure with $\mathcal{C}(\boldsymbol{K},\downarrow) = 3/2$.

4. Trilayer graphene in the presence of electric field

When the trilayer graphene system is exposed to a perpendicular electric field, inversion symmetry breaks in the system and the model Hamiltonian takes the form[46]

$$\mathcal{H}^{\eta}_{s_z}(p) = \frac{v^3p^3}{t_1^2}[\eta\cos(3\phi_{\boldsymbol{p}})\tau_x + \sin(3\phi_{\boldsymbol{p}})\tau_y] + \alpha_{\rm so}\eta\tau_z s_z + \Delta_z\begin{pmatrix}1 & 0\\ 0 & -1\end{pmatrix}. \quad (14)$$

By diagonalizing the above Hamiltonian we gain

$$E_n^{\eta,s_z} = n\sqrt{\left(\frac{v^3p^3}{t_1^2}\right)^2 + (\Delta_z + \alpha_{\rm SO}\eta s_z)^2} = n\varepsilon(p), \quad (15)$$

where $n[=\pm1]$ is the band index with value $+1$ or -1 represents the conduction band and valence band, respectively, and $\varepsilon(p) = \left[(v^3p^3/t_1^2) + (\Delta_z + \alpha_{\rm so}\eta s_z)^2\right]^{1/2}$. We see that the energy of spin $\uparrow$ ($\downarrow$) electron in valley $\boldsymbol{K}$ is not equal to that of spin $\uparrow$ ($\downarrow$) electron in valley $\boldsymbol{K}'$, which is a justification of the statement that the external electric field breaks the inversion symmetry in the trilayer graphene system. It is also quite evident that when $\alpha_{\rm so} > \Delta_z > 0$, the system remains gaped. But when the strength of the applied electric field is increased the gap between spin-up bands gets decreases (Fig. 2(b)) and completely vanishes when the strength of the electric field becomes equal to the ISO coupling strength [see Fig. 2(c)). Thus for the case $\alpha_{\rm so} = \Delta_z$, the trilayer system exhibits a metallic state. When we further increase the applied electric field, the gap between spin-up bands reopens and hence the trilayer graphene goes through a phase transition from QSH state to QVH state [Fig. 2(d)].

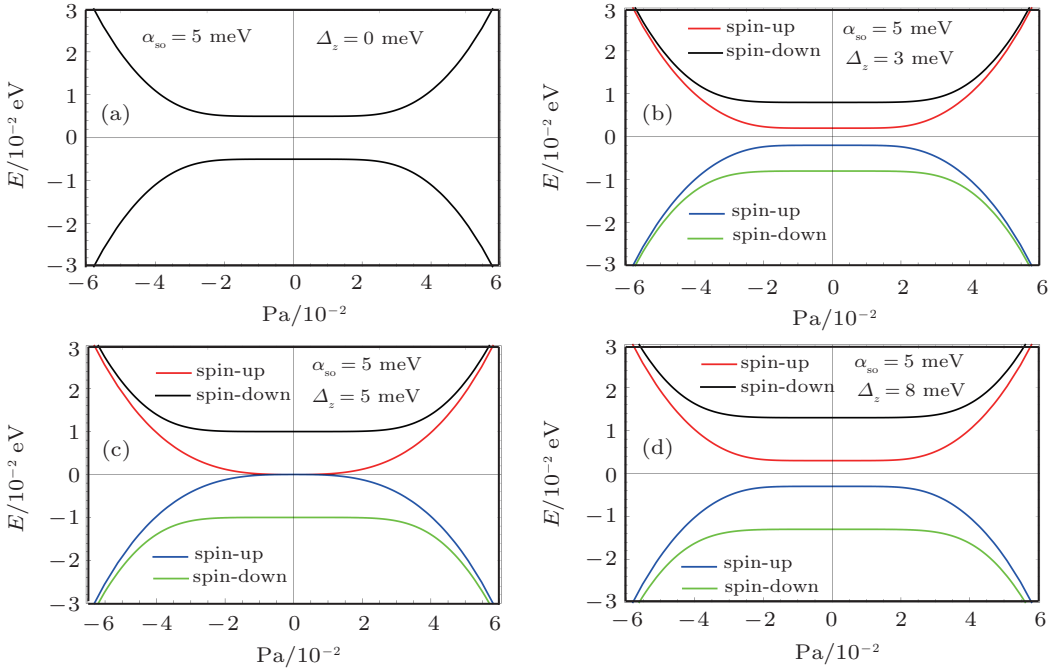


Fig. 2. (color online) Band structure of the trilayer graphene for different values of electric field and ISO coupling. Different values of Δ_z and $\alpha_{\rm so}$ are mentioned inside the plots.

The Hamiltonian (14) can be parameterized in terms of a three-component unit vector $\hat{\boldsymbol{d}}(p)$ as

$$\mathcal{H}^{\eta}_{s_z}(\boldsymbol{p}) = \varepsilon(p)\hat{\boldsymbol{d}}(p)\tau, \quad (16)$$

where the three-component unit vector is defined as

$$\hat{\boldsymbol{d}}(p) = \left[\eta\delta(p)\cos(3\phi_{\boldsymbol{p}}), \delta(p)\sin(3\phi_{\boldsymbol{p}}), \hat{d}_z(p)\right], \quad (17)$$

where $\delta(p) = [1-\hat{d}_z^2(p)]^{1/2}$ and $\hat{d}_z(p) = (\Delta_z + \alpha_{\rm SO}\eta s_z)/\varepsilon(p)$. Repeating the same process as in Section 2, we obtain

$$\mathbb{C}(\eta, s_z) = \frac{3\eta}{2\pi}\int_0^{\infty}\int_0^{2\pi} p\,{\rm d}p\,{\rm d}\phi\,\frac{1}{p}\partial_p\hat{d}_z(p),$$
$$\mathcal{C}(\eta, s_z) = -\frac{3}{2}\eta\hat{d}_z(0) = -\frac{3}{2}\eta\,{\rm sign}(\alpha_{\rm so}\eta s_z + \Delta_z). \quad (18)$$

Hence we find,

$$\mathcal{C} = \sum_{s_z=\pm1}[\mathbb{C}(\eta,\uparrow) + \mathbb{C}(\eta,\downarrow)] = 0,$$
$$\mathcal{C}_s = \sum_{\eta=\pm1}\frac{1}{2}[\mathbb{C}(\eta,\uparrow) - \mathbb{C}(\eta,\downarrow)] = -\frac{3}{2}[{\rm sign}(\alpha_{\rm so} + \Delta_z) + {\rm sign}(\alpha_{\rm so} - \Delta_z)],$$
$$\mathcal{C}_{\rm v} = \sum_{s_z=\pm1}\frac{1}{2}[\mathbb{C}(\eta,\uparrow) - \mathbb{C}(\eta,\downarrow)] = \frac{3}{2}[{\rm sign}(\alpha_{\rm SO} + \Delta_z) - {\rm sign}(\alpha_{\rm SO} - \Delta_z)]. \quad (19)$$

We observe a nice interplay between ISO coupling and external electric field. When $\alpha_{\rm so} > \Delta_z > 0$, we gain $\mathcal{C}_s = -3$

& $\mathcal{C}_{\rm v}=0$, and the system exhibits the QSH state. While for the case $\Delta_z>\alpha_{\rm so}>0$, we obtain $\mathcal{C}_s=0$ & $\mathcal{C}_{\rm v}=3$, and the system exhibits the QVH state. We recover the results of Section 2, when the electric field is switched-off, the corresponding spin/valley Hall conductivity is given by,

$$\sigma_{xy}\,(\text{spin})=\frac{-3e^2}{2h}\left[\text{sign}\,(\alpha_{\rm so}+\Delta_z)+\text{sign}\,(\alpha_{\rm so}-\Delta_z)\right], \quad (20)$$

$$\sigma_{xy}\,(\text{valley})=\frac{3e^2}{2h}\left[\text{sign}\,(\alpha_{\rm so}+\Delta_z)-\text{sign}\,(\alpha_{\rm so}-\Delta_z)\right]. \quad (21)$$

Now, we discuss a more realistic case, when the Fermi level exists in one of the bands. When the Fermi level exists in the conduction band we obtain

$$\begin{aligned}\mathbb{C}\,(\eta,s_z)&=\frac{\eta}{2\pi}\int_0^{p_{\rm F}}\int_0^{2\pi}\mathrm{d}p\mathrm{d}\phi\,\frac{1}{p}\partial_p\hat{d}_z\,(p),\\ \mathbb{C}\,(\eta,s_z)&=\eta\left[\hat{d}_z\,(p_{\rm F})-\hat{d}_z\,(0)\right]\\ &=-\frac{3}{2}\eta\left[\text{sign}\,(\alpha_{\rm so}\eta s_z+\Delta_z)-\hat{d}_z\,(p_{\rm F})\right],\end{aligned}$$

with

$$\begin{aligned}\hat{d}_z\,(p_{\rm F})&=(\Delta_z+\alpha_{\rm SO}\eta s_z)/\varepsilon\,(p_{\rm F}),\\ \varepsilon\,(p_{\rm F})&=\left[(v^3p_{\rm F}^3/t_1^2)+(\Delta_z+\alpha_{\rm SO}\eta s_z)^2\right]^{1/2}.\end{aligned} \quad (22)$$

The spin and valley Hall conductivities become,

$$\sigma_{xy}^{\rm F}\,(\text{spin})=-\frac{3e^2}{h}\left[\frac{\alpha_{\rm so}-\Delta_z}{2\sqrt{(v^3p_{\rm F}^3/t_1^2)+(\alpha_{\rm so}-\Delta_z)^2}}+\frac{\alpha_{\rm so}+\Delta_z}{2\sqrt{(v^3p_{\rm F}^3/t_1^2)+(\alpha_{\rm so}+\Delta_z)^2}}\right], \quad (23)$$

$$\sigma_{xy}^{\rm F}\,(\text{valley})=\frac{3e^2}{h}\left[\frac{\alpha_{\rm so}-\Delta_z}{2\sqrt{(v^3p_{\rm F}^3/t_1^2)+(\alpha_{\rm so}-\Delta_z)^2}}-\frac{\alpha_{\rm so}+\Delta_z}{2\sqrt{(v^3p_{\rm F}^3/t_1^2)+(\alpha_{\rm so}+\Delta_z)^2}}\right]. \quad (24)$$

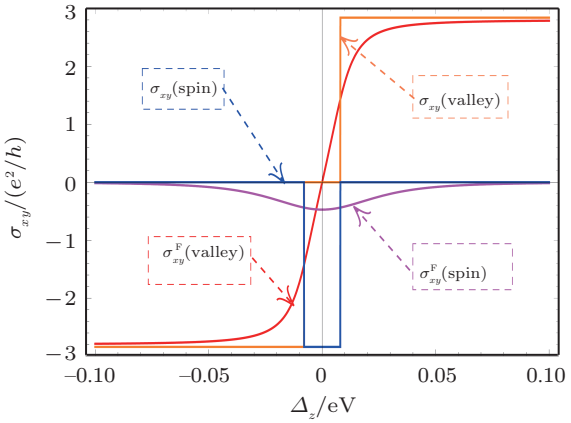


Fig. 3. (color online) Quantum spin/valley Hall conductivities as a function of applied electric field Δ_z for a fixed value of the ISO coupling (4 meV).

We obtain the same results when the Fermi level is in the valence band because of the electron–hole symmetry in our system. We plot Eqs. (23) and (24) in Fig. 3, the QSH/QVH conductivity versus the applied electric field for a fixed-value of ISO coupling. By varying the electric field, we may tune the SHE/VHE. We observe from Fig. 3 that the trilayer graphene also goes through a phase transition in the case when the Fermi level is in the conduction or the valence band.

5. Robustness of QSH state in trilayer graphene against various perturbations

5.1. Rashba spin–orbit interaction

There exists an interesting interplay between RSO coupling and intrinsic SO coupling. The RSO interaction can be induced in the trilayer system by exposing it to a perpendicular electric field or putting on the substrate. By considering both the ISO and RSO coupling effects simultaneously, the two bands Hamiltonian of the trilayer graphene can be modeled as

$$\mathcal{H}^{\eta}\,(p)=\frac{v^3p^3}{t_1^2}[\cos(3\phi_{\boldsymbol{p}})\tau_x+\sin(3\phi_{\boldsymbol{p}})\tau_y]s_0+\alpha_{\rm so}\eta\,\tau_zs_z+2\alpha_{\rm R}\,(\eta\,\tau_xs_y-\tau_ys_x). \quad (25)$$

In matrix form the above Hamiltonian around valley $\boldsymbol{K}$ takes the form

$$\mathcal{H}^{\rm eff}\boldsymbol{K}\,(p)=\begin{pmatrix}\alpha_{\rm so} & 0 & (v^3/t_1^2)\,(p_x-\mathrm{i}p_y)^3 & 0\\ 0 & -\alpha_{\rm so} & \mathrm{i}\alpha_{\rm R} & (v^3/t_1^2)\,(p_x-\mathrm{i}p_y)^3\\ (v^3/t_1^2)\,(p_x+\mathrm{i}p_y)^3 & -\mathrm{i}\alpha_{\rm R} & -\alpha_{\rm so} & 0\\ 0 & (v^3/t_1^2)\,(p_x+\mathrm{i}p_y)^3 & 0 & \alpha_{\rm so}\end{pmatrix}, \quad (26)$$

By diagonalizing the above Hamiltonian, we obtain

$$E_\mu^s\,(p)=\mu\alpha_{\rm R}-s\sqrt{\frac{v^6p^6}{t_1^4}+(\alpha_{\rm so}-\mu\alpha_{\rm R})^2}, \quad (27)$$

where $\mu=\pm1$ represent the conduction $(+)$ band and valence $(-)$ band, respectively. The inclusion of the Rashba spin–orbit coupling mixes up and down spins and thus s_z looses the prop-

erty to be a good quantum number. The resulting eigen-states are then indexed by the spin chirality $s = \pm 1$. We have four branches of the spectrum: two for valence bands and two for conduction bands. Indeed, for the case of $0 < \alpha_R < \alpha_{so}$, the gap remains finite, i.e., $E_g = \sqrt{2}(\alpha_{so} - \alpha_R)$, and hence the trilayer system is a topological insulator [as shown in Fig. 4(a)]. While for the case of $\alpha_R \geqslant \alpha_{so} > 0$, the gap closes and the trilayer graphene converts from a topological state to a zero gap semi-conducting state with cubic dispersive bands [as shown in Fig.4(b)].

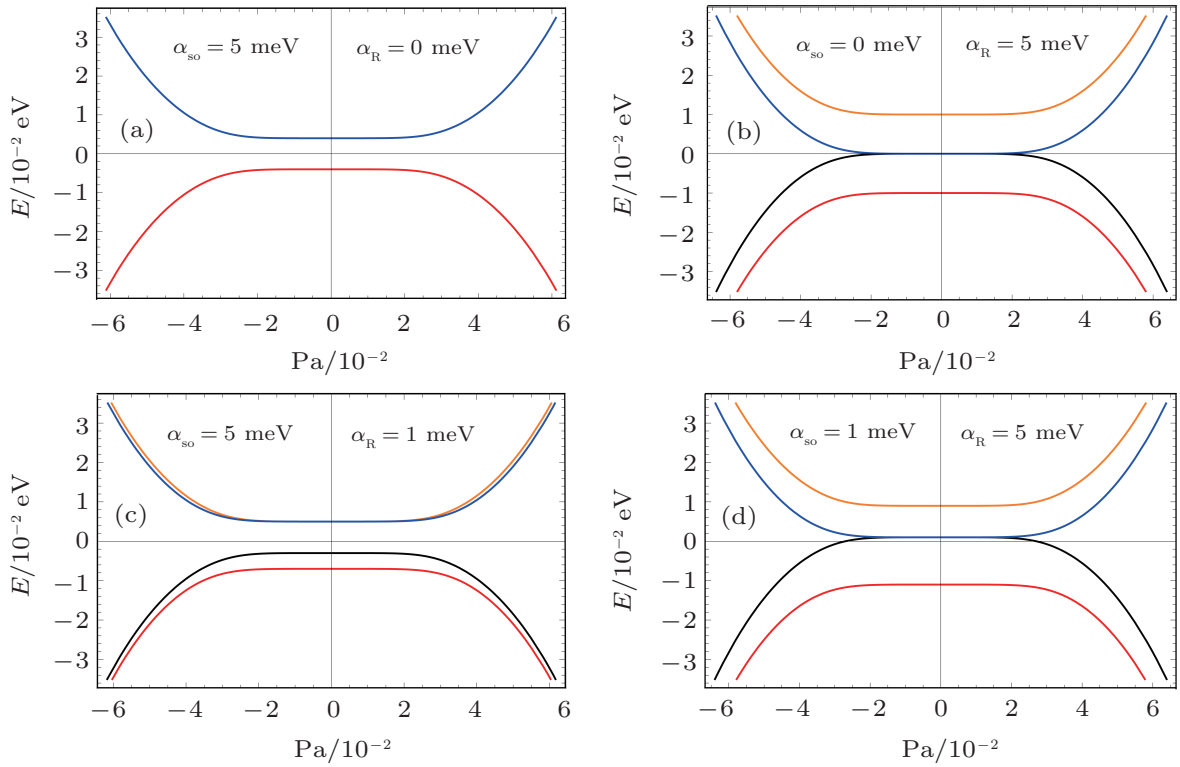


Fig. 4. (color online) (a) The spectrum remains gapped when $\alpha_{so} > \alpha_R > 0$. (b) The spectrum becomes gapless when $\alpha_R \geqslant \alpha_{so} > 0$. The numerical values of α_{so} and α_R are mentioned in the plots.

5.2. Zeeman field

The Hamiltonian of the trilayer graphene in the presence of this new term can be modeled as

$$\mathcal{H}^{\eta}_{s_z}(p) = \frac{v^3 p^3}{t_1^2}\left[\eta\cos(3\phi_{\boldsymbol{p}})\tau_x + \sin(3\phi_{\boldsymbol{p}})\tau_y\right] + \alpha_{so}\eta\tau_z s_z + M s_z \tau_0, \tag{28}$$

where M is the exchange magnetization. By diagonalizing the above Hamiltonian, we obtain

$$E_n^{\eta,s_z} = M s_z + n\sqrt{\left(\frac{v^3 p^3}{t_1^2}\right)^2 + \alpha_{so}^2}, \tag{29}$$

where $n = \pm 1$ represents the conduction $(+1)$ band and valence (-1) band, respectively. The introduction of the exchange field M does not mix up spin and down spin and thus s_z is a good quantum number. The resulting eigen-states are indexed by the spin chirality $s_z = \pm 1$. When the exchange magnetization M is turned on, the lifting of spin-degeneracy occurs in the sense that spin-up $\uparrow$ (spin-down $\downarrow$) bands are pushed upward (down-ward) as shown in Fig. 5. This degeneracy is lifted because of the breaking of TR symmetry and the exchange field is responsible for this. We see another interesting feature for the case of $M > \alpha_{so} > 0$, there exists spin degenerate circles in the momentum space at energy $E_\mu^{s_z} = 0$, that is, taking $E_\mu^s = 0$ in Eq. (28), we can obtain two degenerate circles one for spin $\uparrow$ and one for spin $\downarrow$, which has the following form,

$$p^2 = \left(\frac{M^2 t_1^4}{v^3}\right)^{1/3}.$$

Now the conduction band and the valence band touch each other at some finite momentum instead of at the valley points. The above dispersion (as shown in Fig. 5) shows that for the case $0 < M < \alpha_{so}$, the gap remains finite with a well-defined quantized spin Chern number [as shown in Figs. 5(a) and 5(b)]. This shows that the quantum spin Hall state exists even though the TR symmetry does not preserve in the system; this state is dubbed the TR broken quantum spin Hall state.[13,55] While for the case $M \geqslant \alpha_{so} > 0$, the gap closes and the trilayer graphene converts into a gapless quantum state [as shown in Figs. 5(c) and 5(d)].

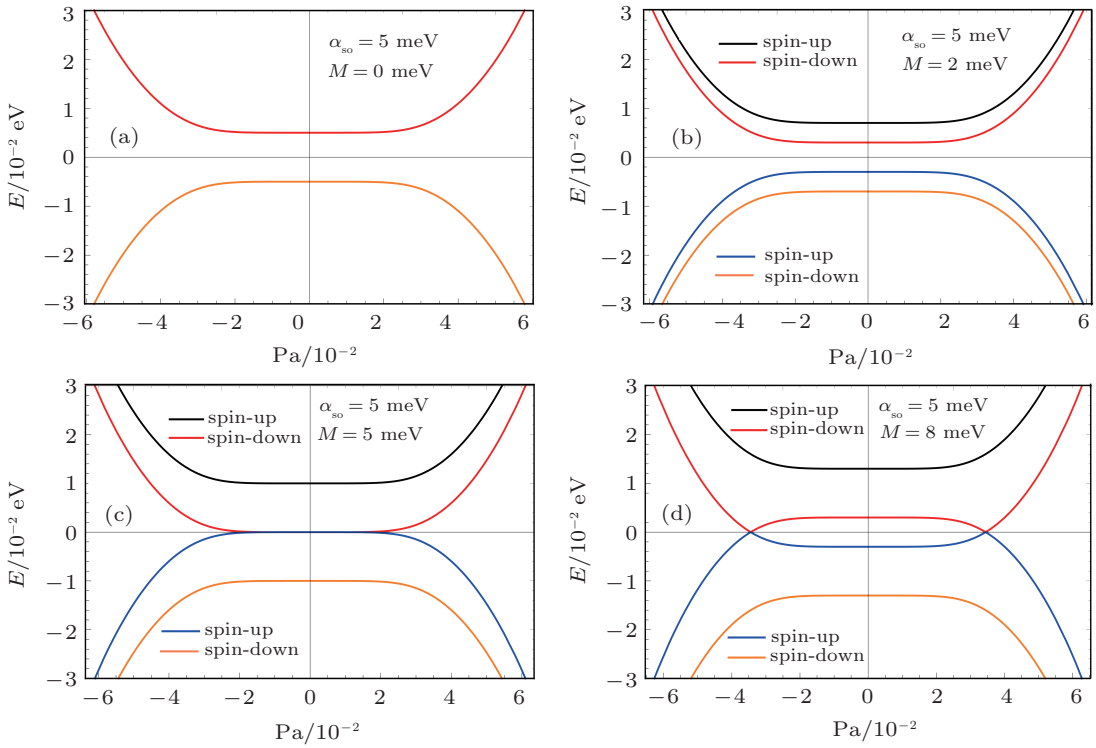


Fig. 5. (color online) (a) The spectrum remains gapped when $\alpha_{so} > M > 0$. The spectrum becomes gapless when (b) $M = \alpha_{so}$ and (c) $M > \alpha_{so} > 0$. The presence of exchange-field M removes the spin-degeneracy, i.e., the spin-up $\uparrow$ (spin-down $\downarrow$) bands move upward (downward). But still there is two-fold spin degeneracy at $E = 0$.

5.3. Trigonal warping

By involving the trigonal effects the Hamiltonian (1) takes the form

$$\mathcal{H}^{\eta}_{s_z}(p) = \mathcal{H}_{\rm el} + \mathcal{H}_{\rm SO} + \mathcal{H}_{\rm w} \tag{30}$$

with

$$\mathcal{H}_{\rm w} = \gamma(p)\begin{pmatrix} 0 & 1 \\ 1 & 0 \end{pmatrix},$$

where $\gamma(p) = t_2/2 - 2vv_3p^2/t_1$ with $v_3 = (\sqrt{3/2})at_3/\hbar$, $t_2(t_3)$ representing coupling between A1 and B3 (A1–B2 and A2–B3) sites. By diagonalization, we obtain,

$$E_n^{\eta,s_z} = n\sqrt{\left(\frac{v^3p^3}{t_1^2}\right)^2 + 2\eta\gamma(p)\frac{v^3p^3}{t_1^2}\cos(3\phi_{\boldsymbol{p}}) + \gamma^2(p) + \alpha_{\rm so}^2}. \tag{31}$$

In contrast to the bilayer graphene, the band gap does not vanish at the valley points even when $\alpha_{\rm SO} = 0$. First we explain the situation when $\alpha_{\rm SO} = 0$. The involvement of this new term in the Hamiltonian affects the energy spectrum around the valley points $\boldsymbol{K}$ and $\boldsymbol{K}'$ in the sense of stretching the iso-energy lines in three directions. In this case the conduction band and valence band do not touch each other at zero momentum ($\boldsymbol{K}$ and $\boldsymbol{K}'$) but at some finite momenta in the direction ϕ.[56] Alternatively, now we have three Dirac points for each valley, where the valence band and conduction band touch other. Here unlike the bilayer graphene, the central Dirac point is missing because $\gamma(p = 0) \neq 0$. When the ISO coupling is switched on, the gap opens at these Dirac points and the system turns out to be an insulator in the bulk. Now to analyze, whether this new term affects the QSH state in trilayer graphene or not, we compute the spin Chern-number.

The Hamiltonian (31) can be parameterized in terms of 3D unit vector $\hat{\boldsymbol{n}}(p)$ as

$$\mathcal{H}^{\eta}_{s_z} = \sum_{i=x,y,z}\sigma_i\hat{n}_i(p), \tag{32}$$

where

$$\hat{n}_x(p) = \gamma(p) + (\eta v^3p^3/t_1^2)\cos(3\phi_{\boldsymbol{p}}),$$
$$\hat{n}_y(p) = (v^3p^3/t_1^2)\sin(3\phi_{\boldsymbol{p}}),$$

and $\hat{n}_z(p) = \alpha_{\rm SO}\eta s_z$. Using Eq. (7), we obtain the same spin Chern-number as in Section 2, i.e., $\mathcal{C}_s = -3$. This shows that the trigonal effects, like the graphene bilayer, do not affect the spin Chern-number. In principle, all the newly designed Dirac points due to trigonal warping, equally contribute in the spin Chern number to make it quantify with the value to be equal to the case with no trigonal effects.

6. SO proximity effects in trilayer graphene

Considering a theoretical model in which only one of the outer layers of the trilayer graphene has a finite intrinsic SO coupling while it is zero in the other two layers. This sort of tenability is un-realizable because the intrinsic SOC is difficult to control from outside like the RSO coupling. However, this model provides a simple theoretical framework to understand

what happens when one considers a coupling between a metal and a topological insulator. For the case in which only one of the layers is affected by the intrinsic SO coupling, the 2×2 Hamiltonian (1) takes the form,

$$\mathcal{H}^{\eta}_{s_z}(p) = \frac{v^3p^3}{t_1^2}\left[\eta\cos(3\phi_{\boldsymbol{p}})\tau_x + \sin(3\phi_{\boldsymbol{p}})\tau_y\right] + \frac{1}{2}\alpha_{\rm so}\eta\left(\sigma_0+\sigma_z\right)s_z. \tag{33}$$

By diagonalizing the above equation, we obtain

$$E_n^{\eta,s_z} = \frac{\alpha_{\rm so}\eta s_z}{2} + \frac{n}{2}\sqrt{\left(\frac{2v^3p^3}{t_1^2}\right)^2 + \alpha_{\rm so}} = \frac{\alpha_{\rm so}\eta s_z}{2} + \frac{1}{2}n\varepsilon(p), \tag{34}$$

where $n=\pm$ with $+1$ (-1) represents the conduction (valence) band. From Eq. (34), we see that the energy for spin $\uparrow(\downarrow)$ electron with valley $\boldsymbol{K}$ does not equal that of a spin $\uparrow(\downarrow)$ electron with valley $\boldsymbol{K}'$, i.e., $E^{\boldsymbol{K},\uparrow}\neq E^{\boldsymbol{K}',\uparrow}$ and $E^{\boldsymbol{K},\downarrow}\neq E^{\boldsymbol{K}',\downarrow}$, this justifies the existence of the inversion asymmetry in the trilayer graphene having intrinsic SO coupling in only one layer. We also observe that $E^{\boldsymbol{K},\uparrow}\neq E^{\boldsymbol{K}',\downarrow}$ and $E^{\boldsymbol{K},\downarrow}\neq E^{\boldsymbol{K}',\uparrow}$, this ensures the TR symmetry in the system. Now combining both of these conditions we concluded that,

$$E^{\boldsymbol{K},\uparrow}\neq E^{\boldsymbol{K},\downarrow},\ \ E^{\boldsymbol{K}',\uparrow}\neq E^{\boldsymbol{K}',\downarrow}. \tag{35}$$

This implies that the energy for each valley depends on the electron spin and is a consequence of the absence of the inversion symmetry in the system. Basically, we have four branches of the spectrum for each valley: two for valence band $(n=-1)$ and two for conduction band $(n=+1)$. From the dispersion relation it looks clear that the two branches are gapless and two have a gap at the Dirac point $(p=0)$, i.e.,

$$\begin{aligned}
\Delta E^{\boldsymbol{K}}(p=0) &= \left|E^{\boldsymbol{K}}_{+,\downarrow} - E^{\boldsymbol{K}}_{-,\uparrow}\right| = 0,\\
\Delta E^{\boldsymbol{K}'}(p=0) &= \left|E^{\boldsymbol{K}'}_{+,\uparrow} - E^{\boldsymbol{K}'}_{-,\downarrow}\right| = 0,\\
\Delta E^{\boldsymbol{K}}(p=0) &= \left|E^{\boldsymbol{K}}_{+,\uparrow} - E^{\boldsymbol{K}}_{+,\downarrow}\right| = \lambda_{\rm so},\\
\Delta E^{\boldsymbol{K}'}(p=0) &= \left|E^{\boldsymbol{K}'}_{+,\downarrow} - E^{\boldsymbol{K}'}_{+,\uparrow}\right| = \lambda_{\rm so}.
\end{aligned} \tag{36}$$

All these bands are plotted in Fig. 6. Now the Hamiltonian (33) can be parameterized in terms of a three-component unit vector $\hat{\boldsymbol{d}}(p)$ as

$$\tilde{\mathcal{H}}^{\rm eff}_{s_z}\eta(\boldsymbol{p}) = \varepsilon(\boldsymbol{p})\left[\tau_x\hat{d}_x(\boldsymbol{p}) + \tau_y\hat{d}_y(p) + (\tau_0+\tau_z)\hat{d}_z(\boldsymbol{p})\right], \tag{37}$$

where the three-component unit vector is defined as

$$\hat{\boldsymbol{d}}(p) = \left[\eta\delta(\boldsymbol{p})\cos(3\phi_{\boldsymbol{p}}), \delta(\boldsymbol{p})\sin(3\phi_{\boldsymbol{p}}), \hat{d}_z(\boldsymbol{p})\right], \tag{38}$$

where $\delta(p) = [1-\hat{d}_z^2(p)]^{1/2}$ and $\hat{d}_z(p) = \alpha_{\rm SO}\eta s_z/\varepsilon(p)$. The form of the unit vector $\hat{\boldsymbol{d}}(p)$ is similar to that of the trilayer graphene with SO coupling in both layers and hence this system will have the same Chern-number as that of the trilayer graphene with SO coupling in both layers, i.e., $\mathcal{C}(\eta, s_z) = -s_z$. But this result goes against our dispersion relation (34) which shows that our system is not a true insulator at all but an indirect zero gap semiconductor [see Fig. 6]. From Fig. 6, we see that when both spins and (or) both valleys are taken into account then the spectrum becomes gapless. However, it is clear that for each spin and valley we have an energy gap equal to $\alpha_{\rm so}$ at $p=0$:

$$\begin{aligned}
\Delta E^{\boldsymbol{K},\uparrow}(p=0) &= \left|E^{\boldsymbol{K}}_{+,\uparrow} - E^{\boldsymbol{K}}_{-,\uparrow}\right| = \alpha_{\rm so},\\
\Delta E^{\boldsymbol{K},\downarrow}(p=0) &= \left|E^{\boldsymbol{K}}_{+,\downarrow} - E^{\boldsymbol{K}}_{-,\downarrow}\right| = \alpha_{\rm so},\\
\Delta E^{\boldsymbol{K}',\uparrow}(p=0) &= \left|E^{\boldsymbol{K}'}_{+,\uparrow} - E^{\boldsymbol{K}'}_{-,\uparrow}\right| = \alpha_{\rm so},\\
\Delta E^{\boldsymbol{K}',\downarrow}(p=0) &= \left|E^{\boldsymbol{K}'}_{+,\downarrow} - E^{\boldsymbol{K}'}_{-,\downarrow}\right| = \alpha_{\rm so},
\end{aligned}$$

Thus, we conclude that the trilayer graphene with only one layer having the essence of the ISO coupling is not a quantum spin Hall system because of having the gapless bulk spectrum.

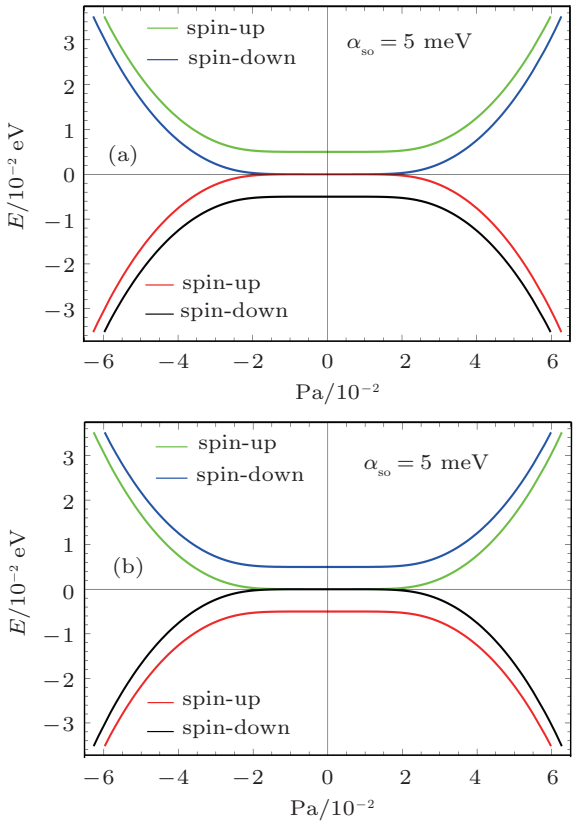


Fig. 6. (color online) Low energy spectrum of the trilayer graphene with only one layer has the essence of ISO interaction. Panel (a) (panel (b)) corresponds to the bands near valley $\boldsymbol{K}$ ($\boldsymbol{K}'$). The introduction of intrinsic SO coupling in only layer opens an energy gap having an amount of $\alpha_{\rm so}$ with different signs for spin-up $\uparrow$ and spin-down $\downarrow$ as well as for valley $\boldsymbol{K}$ and $\boldsymbol{K}'$.

7. Summary

In conclusion, we studied the two bands low energy description of the ABC trilayer graphene system in the presence

of the intrinsic SO coupling to probe as a topological insulator. Our results show that the trilayer graphene goes through a phase transition from zero gap semiconductor to a QSH phase when the intrinsic SO coupling is introduced. We analytically calculated that the net spin Chern number for each spin in the trilayer graphene system is three times that of the single layer graphene. This confirms that the trilayer graphene has triple edge states as compared to a single layer. The spin Chern number is odd, which confirms that our proposed system is a strong topological insulator. The band topology of the trilayer graphene was also discussed by plotting $\hat{\boldsymbol{d}}(p)$ as a function of momentum $\boldsymbol{p}$ over a unit sphere, which shows that $\hat{\boldsymbol{d}}(p)$ displays a triple-vortex meron-like configuration for each spin and valley. Besides, we found that the trilayer graphene system goes through a phase transition from QSH state to QVH state, in the presence of the electric field. In addition, we introduced various perturbations such as Rashba SO coupling and Zeeman field, and investigated the stability of the QSH phase; in the presence of these perturbations, the following results were obtained: (i) non-trivial topological phase when $\alpha_{\rm so} > (\alpha_{\rm R}, \Delta_z, M) > 0$; (ii) the QVH phase when $\Delta_z > \alpha_{\rm so} > 0$; (iii) the metallic state when $(\alpha_{\rm R}, M) \geqslant \alpha_{\rm so} > 0$. Besides this, we investigated that the trigonal warping does not affect the spin Chern number.

Moreover, we considered a situation in the trilayer graphene in which only one of the out layers has the essence of the intrinsic SO coupling. Although the nonzero Chern number for each valley signals that the system is a topological insulator, but in fact, it is not a topological insulator because the spectrum of the system is not gapped as a whole.

Acknowledgments

The author Majeed Ur Rehman acknowledges the support from the Chinese Academy of Sciences (CAS) and TWAS for his Ph. D. studies at the University of Science and Technology, China in the category of 2016 CAS-TWAS President's Fellowship Awardee (Grant No. 2016-156).

References

[1] Qi X L and Zhang S C 2011 *Rev. Mod. Phys.* **83** 1057
[2] Klitzing K V 1985 *Nobel Lecture: The Quantized Hall Effect*
[3] Klitzing K V, Dorda G and Pepper M 1980 *Phys. Rev. Lett.* **45** 494
[4] Bansil A, Lin H and Das T 2016 *Rev. Mod. Phys.* **88** 021004
[5] Hasan M Z and Kane C L 2010 *Rev. Mod. Phys.* **82** 3045
[6] Xiao G L, Gu F Z, Guang F W, Hua C, Culcer D and Zhen Y Z 2013 *Chin. Phys. B* **22** 097306
[7] Wang J and Zhu B F 2013 *Chin. Phys. B* **22** 067301
[8] Thouless D J, Kohmoto M, Nightingale M P and Nijs M D 1982 *Phys. Rev. Lett.* **49** 405
[9] Haldane F D M 1988 *Phys. Rev. Lett.* **61** 2015
[10] Kane C L and Mele E J 2005 *Phys. Rev. Lett.* **95** 146802
[11] Kane C L and and Mele E J 2005 *Phys. Rev. Lett.* **95** 226801
[12] Buhmanna H 2011 *J. Appl. Phys.* **109** 102409
[13] Li S, Chao L H You Y Y, Ning S D and Yu X D 2013 *Chin. Phys. B* **22** 067201
[14] Ming G H and Ping F S 2012 *Chin. Phys. B* **21** 077303
[15] Ming G H, Lin Z X and Ping F S 2012 *Chin. Phys. B* **21** 0117301
[16] Gmitra M, Konschuh S, Ertler C, Draxl C A and Fabian J 2009 *Phys. Rev. B* **80** 235431
[17] Fu L and Kane C L 2006 *Phys. Rev. B* **74** 195312
[18] Chang M C and Niu Q 1995 *Phys. Rev. Lett.* **75** 1348
[19] Sheng D N, Weng Z Y, Sheng L and Haldane F D M 2006 *Phys. Rev. Lett.* **97** 036808
[20] Park H and Marzari N 2011 *Phys. Rev. B* **84** 205440
[21] Min H, Hill J E, Sinitsyn N A, Sahu B R, Kleinman L and MacDonald A H 2006 *Phys. Rev. B* **74** 165310
[22] YaoY G, Ye F, Qi X L, Zhang S C and Fang Z 2007 *Phys. Rev. B* **75** 041401
[23] Konig M, Wiedmann S, Brune C, Roth A, Buhmann H, Molenkamp LW, Qi X L and Zhang S C 2007 *Science* **318** 766
[24] Bernevig B A, Hughes T L and Zhang S C 2006 *Science* **314** 1757
[25] Tahir M, Manchon A, Sabeeh K and Schwingenschlogl U 2013 *Appl. Phys. Lett.* **102** 162412
[26] An X T, Zhang Y Y, Liu J J and Li S S 2013 *Appl. Phys. Lett.* **102** 043113
[27] Xiao A D, Yao W and Niu Q 2007 *Phys. Rev. Lett.* **99** 236809
[28] Qiao Z, Tse W K, Jiang H, Yao Y and Niu Q 2011 *Phys. Rev. Lett.* **107** 256801
[29] Pan C H, Li Z, Liu C C, Zhu G, Qiao Z and Yao Y 2014 *Phys. Rev. Lett.* **112** 106802
[30] Yang F, Wang H L and Pan H 2017 *Chin. Phys. B* **26** 017102
[31] Yu T H 2015 *Chin. Phys. B* **24** 127301
[32] Mei Z, Wei W L, Jun D and Ying Z 2015 *Acta Phys. Sin.* **64** 107301
[33] Wang K, Ren Y, Deng X, Yang S A, Jung J and Qiao Z 2017 *Phys. Rev. B* **95** 245420
[34] Deng X, Qi S, Han Y, Zhang K, Xu X and Qiao Z 2017 *Phys. Rev. B* **95** 121410
[35] Xu B, Li R and Fu H H 2017 *Chin. Phys. B* **26** 057303
[36] Lu H Z and Shen S Q 2016 *Chin. Phys. B* **25** 0117202
[37] Zheng Y J, Song J T and Li Y X 2016 *Chin. Phys. B* **25** 037301
[38] Zeng J, Ren Y, Zhang K and Qiao Z 2017 *Phys. Rev. B* **95** 045420
[39] Zhang J, Zhao B, Zhou T and Yang Z 2016 *Chin. Phys. B* **25** 117308
[40] Qiao Z, Han Y, Zhang L, Wang K, Deng X, Jiang H, Yang S A, Wang J and Niu Q 2016 *Phys. Rev. Lett.* **117** 056802
[41] Ren Y, Zeng J, Deng X, Yang F, Pan H and Qiao Z 2016 *Phys. Rev. B* **94** 085411
[42] Kormanyos A and Burkard G 2013 *Phys. Rev. B* **87** 045419
[43] Klinovaja J, Ferreira G J and Loss D 2012 *Phys. Rev. B* **86** 235416
[44] Castro Neto A H and Guinea F 2009 *Phys. Rev. Lett.* **103** 026804
[45] Konschuh S, Gmitra M, Kochan D and Fabian J 2012 *Phys. Rev. B* **85** 115423
[46] Prada E, Jose P S, Brey L and Fertig H A 2011 *Solid State Commun.* **151** 1075
[47] Yuan S, Roldan R and Katsnelson M I 2011 *Phys. Rev. B* **84** 125455
[48] Zhang F, Sahu B, Min H and MacDonald A H 2010 *Phys. Rev. B* **82** 035409
[49] Min H, Hill J E, Sinitsyn N A, Sahu B R, Kleinman L and MacDonald A H 2006 *Phys. Rev. B* **74** 165310
[50] Girvin S M and MacDonald A H 1997 *Perspectives in Quantum Hall Effects* (Wiley-Interscience)
[51] Volovik G E 2017 *Low Temperature Physics* **43** 47
[52] Zvyagin A A 2016 *Low Temperature Physics* **42** 971
[53] Sinitsyn N A, Hill J E, Min H, Sinova J and MacDonald A H 2006 *Phys. Rev. Lett.* **97** 106804
[54] Schroeter D S and Garst M 2015 *Low Temperature Physics* **41** 817
[55] Yang Y, Xu Z, Sheng L, Wang B, Xing D Y and Sheng D N 2011 *Phys. Rev. Lett.* **107** 066602
[56] Koshino M and McCann E 2009 *Phys. Rev. B* **80** 165409